Published in final edited form as:
J Cell Physiol. 2012 April ; 227(4): 1776–1785. doi:10.1002/jcp.22911.

Requirements for Ion and Solute Transport, and pH Regulation During Enamel Maturation

RODRIGO S. LACRUZ[1,*], **CHARLES E. SMITH**[2], **PIERRE MOFFATT**[3], **EUGENE H. CHANG**[4], **TIMOTHY G. BROMAGE**[5], **PABLO BRINGAS JR.**[1], **ANTONIO NANCI**[6], **SANJEEV K. BANIWAL**[7], **JOSEPH ZABNER**[8], **MICHAEL J. WELSH**[8], **IRA KURTZ**[9], and **MICHAEL L. PAINE**[1,*]

[1]Center for Craniofacial Molecular Biology, Herman Ostrow School of Dentistry, University of Southern California, Los Angeles, California

[2]Facility for Electron Microscopy Research, Department of Anatomy and Cell Biology and Faculty of Dentistry, McGill University, Montreal, Quebec, Canada

[3]Genetics Unit, Shriners Hospital for Children, Montreal, Quebec, Canada

[4]Department of Otolaryngology, Roy J. and Lucille A. Carver College of Medicine, University of Iowa, Iowa City, Iowa

[5]Department of Biomaterials and Biomimetics, New York University College of Dentistry, New York, New York

[6]Laboratory for the Study of Calcified Tissues and Biomaterials, Faculté de Médecine Dentaire, Université de Montréal, Montreal, Quebec, Canada

[7]Department of Biochemistry and Molecular Biology, Keck School of Medicine, University of Southern California, Los Angeles, California

[8]Department of Internal Medicine, Roy J. and Lucille A. Carver College of Medicine, University of Iowa, Iowa City, Iowa

[9]David Geffen School Medicine at the University of California at Los Angeles, Los Angeles, California

Abstract

Transcellular bicarbonate transport is suspected to be an important pathway used by ameloblasts to regulate extracellular pH and support crystal growth during enamel maturation. Proteins that play a role in amelogenesis include members of the ABC transporters (SLC gene family and CFTR). A number of carbonic anhydrases (CAs) have also been identified. The defined functions of these genes are likely interlinked during enamel mineralization. The purpose of this study is to quantify relative mRNA levels of individual SLC, Cftr, and CAs in enamel cells obtained from secretory and maturation stages on rat incisors. We also present novel data on the enamel phenotypes for two animal models, amutant porcine(CFTR-ΔF508) and the NBCe1-null mouse.Our data show that two SLCs(AE2 and NBCe1),*Cftr*,and Car2, Car3,Car6,and Car12 are all significantly up-regulated at the onset of the maturation stage of amelogenesis when compared to the secretory stage. The remaining SLCs and CA gene transcripts showed negligible expression or no

[*]Correspondence to: Rodrigo S. Lacruz and Michael L. Paine, Center for Craniofacial Molecular Biology, Herman Ostrow School of Dentistry, University of Southern California, 2250 Alcazar Street, CSA Room #103, Los Angeles, CA 90033. rodrigo@usc.edu, paine@usc.edu.

All authors have no conflicts of interest.

significant change in expression from secretory to maturation stages. The enamel of *Cftr*-ΔF508 adult pigs was hypomineralized and showed abnormal crystal growth. NBCe1-null mice enamel was structurally defective and had a marked decrease in mineral content relative to wild-type. These data demonstrate the importance of many non-matrix proteins to amelogenesis and that the expression levels of multiple genes regulating extracellular pH are modulated during enamel maturation in response to an increased need for pH buffering during hydroxyapatite crystal growth.

Many diseases and multiple organ pathologies are directly related to abnormalities in pH regulation and ion transport. These may result from mutations in genes encoding ion transporters (e.g., solute carriers or *SLC* gene products), chloride channels (e.g., CFTR), or carbonic anhydrases (e.g., CA2). Three examples of these diseases are proximal renal tubular acidosis (pRTA) from *SLC4A4* mutations (Igarashi et al., 1999; Dinour et al., 2004; Inatomi et al., 2004; Demirci et al., 2006; Gawenis et al., 2007), cystic fibrosis (CF) from *Cftr* mutations (Welsh and Smith, 1993; Sheppard and Welsh, 1999), and osteopetrosis from *CA2* mutations (Venta et al., 1991; Aramaki et al., 1993). The expression and biochemical role of many of these gene products in organs other than teeth is well understood but their significance in enamel development is now emerging.

The SLC superfamily of solute carrier membrane proteins have many important functions in eukaryote biology. These transporters act as the cell's gatekeepers and comprise several active and passive transporters that control uptake and efflux of many critical ions/substrates (Hediger et al., 2004). The plasma membrane SLC gene products that are expressed in ameloblasts include AE1, AE2, NBCe1, NHE1, NCX1, and NCX3 (Lyaruu et al., 2008; Paine et al., 2008; Bronckers et al., 2009; Josephsen et al., 2010; Okumura et al., 2010; Lacruz et al., 2010c; Urzua et al., 2011), and all participate in bicarbonate (HCO_3^-), H^+ or Ca^{2+} transport (Hediger et al., 2004; Josephsen et al., 2010; Lacruz et al., 2010b). Carbonic anhydrases (CA) catalyze the reversible conversion of CO_2 to bicarbonate (HCO_3^-). There are 16 recognized CA genes in the mouse genome and these encompass mitochondrial, cytoplasmic, plasma membrane-bound and secreted isoforms that are either catalytically active (13 isozymes) or acatalytic (3 isoforms; Fujikawa-Adachi et al., 1999; Chegwidden et al., 2000; Supuran, 2008a,b). The three acatalytic CA isoforms (CA8, CA10, and CA11) are also referred to as CA-related proteins (CA-RP). Multiple isoforms from an individual CA gene (e.g., alternative spliced isoforms or alternate promoter usage) have not been recognized. In addition, protein tyrosine phosphatase receptor type B (Ptprb; Peles et al., 1995) and Ptprg (Wary et al., 1993) each contain a CA-like domain, and have previously been described as CA-RP.

Maintenance of pH homeostasis of the mineralizing enamel matrix environment is essential for building normal enamel (Lacruz et al., 2010b). During the final stage of enamel mineralization, when enamel crystals become fully mature by markedly increasing in volume, the extracellular pH drops (Smith et al., 1996), and unless (HCO_3^-) is generated or transported to this region, a continued acidification of pH may inhibit further mineralization (Simmer and Fincham, 1995), and eventually be toxic to the cells. Mineral transport to the enamel is also required for proper crystal growth. With this knowledge, we initiated this study to show how (HCO_3^-) may be delivered to, or produced within, the enamel matrix to ensure that the extracellular acid–base milieu is conducive to mineralization. Furthermore, we had previously reported on the enamel phenotype of NBCe1-null mice and the deciduous dentition of *Cftr*-ΔF508 pigs. Here, we present novel data on the permanent dentition of *Cftr*-ΔF508 pigs and describe in more detail the enamel microstructure of NBCe1-null mice using Field Emission Microscopy. We also compared mineral content of wild-type (WT) and NBCe1-null mice using Energy Dispersive X-Ray Spectroscopy (EDAX).

Materials and Methods

Animals

All vertebrate animal manipulation complied with Institutional and Federal guidelines.

NBCe1-null animals and animal husbandry

Complete details of the NCBe1$^{+/-}$ and NBCe1$^{-/-}$ (Gawenis et al., 2007) animal husbandry, breeding, and genotyping has been reported (Lacruz et al., 2010c).

CFTR-mutant (CFTR-ΔF508) pigs

A 12-month-old *Cftr*-ΔF508 pig (Rogers et al., 2008a,b; Stoltz et al., 2010) was euthanized and the teeth were immediately dissected and immersed in ethanol. The teeth from a 6-month-old WT domestic pig were collected for comparison. At 6 months, the domestic pig has a mixed dentition with the crowns of the permanent first molars fully formed and with some root developed. Previously we had examined a fully erupted deciduous mandibular third incisor of a newborn *Cftr*-ΔF508 pig and showed enamel hypomineralization when compared to an age-matched control (Chang et al., 2011). Here, we compare the permanent dentition of a CF mutant animal and a non-affected control. Data are presented for the fully erupted distal–palatal cusp of the permanent maxillary left first molar for both the *Cftr*-ΔF508 (CF mutant) and WT (control) pigs.

Scanning electron microscope

The mandibles of 14-day-old NBCe1$^{-/-}$ and WT littermate control mice were dissected and cleaned of soft tissues and kept at 4°C in 70% ethanol. Hemi-mandibles of WT and NBCe1 $^{-/-}$ animals were dehydrated in ethanol series and embedded in polymethylmethacrylate (PMMA) resin and cut with a diamond band saw at a point just below the erupted tip of the incisor to obtain a representative cross-section of the fully mature enamel. Each PMMA block was subsequently polished to a surface finish of 1 μm and acid etched (37% phosphoric acid) for 3 sec. Specimens were washed, air dried, and imaged at variable vacuum (50 Pa) by backscattered electron microscopy in the scanning electron microscope (BSE-SEM) using a Zeiss EVO-50 at 15 kV and 200 pA without a conductive coating. The same method was used to prepare the *Cftr*-null pig permanent maxillary molars. The electron beam was confirmed stable after 30 min of operation and, when possible, BSE detection, contrast, and brightness were arbitrarily set to conditions that contained both specimens within a broad 0–255 grey dynamic range for semi-quantitative comparison. When mineralization density differences between WT and experimental specimens were too large to be sensibly contained within the full dynamic range, representative images were acquired for illustrative purposes. The *Cftr*-ΔF508 pig molars and the NBCe1-null mice gray-level images were subject to an 8-bin color look-up-table for visual comparison of differences in mineralization density between samples. Following BSE-SEM imaging of *Cftr*-ΔF508 pig molars, the samples were lightly coated with gold to be imaged in secondary electron emission mode by field emission scanning electron microscopy (below).

Field emission microscopy and EDAX

The lower incisors of 15-day-old NBCe1-null mice and WT littermates were dissected out and air-dried before mechanically fracturing the tooth coronally near the incisal tip. The specimens were mounted on SEM stubs and carbon coated for 6 sec to be examined by field emission scanning electron microscopy (FE-SEM; JEOL JSM-7001) with EDAX capability operated in secondary electron mode at 10 kV in high vacuum. Two WT and 2 NBCe1 $^{-/-}$ animals were analyzed. Three different zones of the enamel were sampled for each incisor of

each animal to obtain an average value for WT and NBCe1 $^{-/-}$ mice. We combined map scanning in areas of about 40 μm in width with spot scans in WT and NCBe1 $^{-/-}$ samples. Pig molars were also examined by FE-SEM (Carl Zeiss NTS, LLC North America) in secondary electron emission mode at 0.5 kV in high vacuum.

Rat tissue dissection

Ten adult male Wistar Hannover rats weighing 170–190 g were euthanized and their mandibles were immediately dissected out, the surrounding soft tissues removed, and the mandibles frozen in liquid nitrogen as previously described (Smith et al., 2006). Mandibles were kept in liquid nitrogen overnight and the samples were then lyophilized for 24 h. The mandibular bone encasing the lower incisors was carefully removed to expose the entire labial surface. Enamel organ cells were collected by gentle scraping from three different regions of the incisor (Fig. 1). A molar reference line was used to isolate cells from secretory, early-mid maturation, and mid-late maturation stages, following the method previously described by Smith and Nanci (1989), but adapted here for rats weighing 170–190 g. Pooled tissues from 10 rats were used to ensure adequate mRNA for the execution of the entire experiment.

Total RNA isolation and real-time PCR

Total RNA was extracted by homogenizing the freeze-dried cells from each of the three zones using Qiagen RNeasy Minikit. Reverse-transcribed PCR was performed using iScript cDNA Synthesis kit Thermal (Bio-Rad Life Sciences, Hercules, CA). Quantitative real-time PCR (qPCR) reactions were performed using iQ™ SYBR® Green Supermix (BioRad) using primer pairs shown in Table 1. All primer pairs were designed to span intronic regions, and are the rat-equivalent to either human or mouse primer pairs identified in “Primer Bank” and are ideal for qPCR (http://pga.mgh.harvard.edu/primerbank/index.html). Relative expression of mRNA was calculated using the delta delta C_T method (Livak and Schmittgen, 2001). All values for the mRNA species were initially assessed/normalized to both β-actin and Gapdh, however, negligible variability between mRNA levels (secretory, early maturation, and late maturation stage) was noted for β-actin (Gapdh showed small but significant up-regulation in maturation stage), thus all data presented was normalized to β-actin. All qPCR samples were run in triplicate, and standard deviations calculated and included in the graphs. Statistically significant changes ($P < 0.05$) in gene expression were determined using the two-tailed Student’s *t*-test.

Results

NBCe1-null mice

NBCe1-null mice have been previously analyzed for enamel defects (Lacruz et al., 2010c). Here, BSE-SEM images from 14-day-old NBCe1-null (NBCe1 $^{-/-}$) mouse incisors clearly show a thinner than normal enamel layer and severe enamel hypomineralization when compared to WT incisors of the same inbred strain (Fig. 2C as compared to Fig. 2A). NBCe1-null (Gawenis et al., 2007) mice are maintained and bred in the Black Swiss genetic background. We have stated previously that the NBCe1 $^{-/-}$ enamel architecture was abnormal, and that the “enamel hardness of NBCe1 $^{-/-}$ animals was not measurable, due to the extreme softness and fragility of the tissue” (Lacruz et al., 2010c). To obtain comparative density-dependent BSE-SEM images of WT and experimental specimens, we stabilized beam parameters and established stage coordinates for each field of view for all specimens prior to image capture. In this way, rapid computer control of stage movements from one specimen to the other allowed us to acquire images under identical imaging parameters (e.g., magnification, brightness, contrast, etc.) within seconds of each other. Thus brightness levels for WT and NBCe1 $^{-/-}$ mice can be used to generate color-coded images to

compare differences in mineralization. As observed in Figure 2B,D, NBCe1 $^{-/-}$ mice present hypomineralized enamel when compared with a WT littermate. The mineralization of the enamel in NBCe1 $^{-/-}$ null mice is comparable to that of the dentine imaged in WT.

We next analyzed details of the enamel composition and microstructure of NBCe1 $^{-/-}$ mice by Field Emission Microscopy equipped with EDAX enabling us to compare relative differences in mineral content between NBCe1 $^{-/-}$ and WT mice. Spot and map scanning showed minor differences which were ≤3%. Results show that NBCe1 $^{-/-}$ mice have markedly lower levels of calcium and phosphorus when compared with WT littermates, showing a decrease of 46% (Ca^{2+}) and 40% (P^{3-}). The ratios of Ca^{2+}/P^{3-} were lower in NBCe1 $^{-/-}$ animals (1.7) relative to WT (1.9). Sodium levels were 21% lower in NBCe1 $^{-/-}$ animals, whereas chloride levels had decreased by 90% compared to WT. In contrast, Mg^{2+} levels were higher in NBCe1 $^{-/-}$ animals by about 10%. Figure 3 shows that the enamel microstructure of NBCe1 $^{-/-}$ mice in FE-SEM showing a heavily disrupted tissue lacking proper rod–interrod boundaries and presenting abnormal crystal formation.

CFTR-ΔF508 pigs have a hypomineralized enamel phenotype

In an earlier studies (Chang et al., 2011) we examined the enamel of deciduous incisor teeth (mandibular Di3) from both *Cftr*-ΔF508 and *Cftr*-null pigs, which showed a "hypomineralized enamel when compared to WT animals." Here we compared the permanent dentition of *Cftr*-ΔF508 and WT pigs. Figure 4 shows BSE-SEM (Parts A, B, D, E) images of the permanent molars. The *Cftr*-ΔF508 pig enamel (Parts D and E) is hypomineralized when compared to a WT pig (Parts A and B). Parts C and F show high magnification images of the lateral enamel of WT and *Cftr*-ΔF508 pig molars by FE-SEM operated in secondary electron emission mode. The enamel crystallites of the *Cftr*-ΔF508 pig are visibly disorganized (Part F) when compared with WT (Part C). Figure 4 also shows that the cusp of the *Cftr*-ΔF508 animal presents patches of mineralized enamel being of similar density to normal enamel. The lateral enamel is much less mineralized and more closely resembling the mineral density of dentine, suggesting a possible gradient of mineralization related to crown development over time in the *Cftr*-ΔF508 pig.

Confirmation of dissection accuracy by defining stages of amelogenesis using enamel-specific gene transcripts

Total RNA was prepared from three cell populations derived from the enamel organ of 10 male Wistar Hannover rats. These cell populations were obtained from secretory, early-mid maturation, and mid-late maturation stages of amelogenesis as illustrated in Figure 1. Gene transcripts shown in many studies to have high or low expression patterns depending on the developmental stage sampled and are limited to ameloblasts, were chosen to assess the accuracy of the cell dissections. Amelogenin (Amelx) and enamelin (Enam) are products of secretory and early maturation stage ameloblasts, and their expression is low or not apparent during late maturation stages of amelogenesis (Hu et al., 2001). Odontogenic ameloblast associated protein (Odam) is a product of maturation stage ameloblasts, and expression is low or not apparent during secretory stage amelogenesis (Moffatt et al., 2008). All data were normalized to β-actin (Actb).

Our results confirm that we were able to accurately dissect these three stages of amelogenesis by showing high Amelx and Enam mRNA expression in secretory stage, a sharp decline in their mRNA levels during the early-mid maturation stage, and barely detectable mRNA levels during the mid-late maturation stages (Fig. 5, Parts A and B). At all three stages of amelogenesis the changes noted for Amelx and Enam were statistically significant ($P < 0.05$). In contrast, Odam is most highly expressed in ameloblasts during the maturation stages, although negligible expression is noted in the secretory stage (Fig. 5, Part

B), and this change in expression from secretory to early-mid and mid-late maturation stages was statistically significant $P < 0.05$).

Changes to AE2, NBCe1, and Cftr expression

The biochemical functions of AE1, AE2, NBCe1, Cftr, and NHE1 in ameloblasts have been discussed previously (Sui et al., 2003; Paine et al., 2008; Bronckers et al., 2010; Josephsen et al., 2010; Lacruz et al., 2010a,b,c; Simmer et al., 2010). In this study, we wanted to assess changes in the relative expression levels for each gene transcript at the various stages of amelogenesis using qPCR. AE2, NBCe1, and Cftr showed a significant up-regulation (2.9-, 3.4-, and 5.6-fold increases respectively) in mid-late maturation stage amelogenesis when compared to secretory stage amelogenesis (Fig. 6). The results for AE1 and NHE1 were less remarkable. AE1 showed significant gene down-regulation, while levels for NHE1 remained relatively constant in a similar comparison (Fig. 6). Our results confirm previous findings that AE2, NBCe1, and Cftr are expressed in enamel organ cells during amelogenesis. Our data also confirms that significant levels of AE1 and NHE1 are also present in enamel cells. This increased expression of AE2 (Lyaruu et al., 2008; Bronckers et al., 2009), NBCe1 (Paine et al., 2008; Lacruz et al., 2010c), and Cftr (Wright et al., 1996b; Sui et al., 2003; Chang et al., 2011) during enamel maturation highlights the greater requirement for ameloblast bicarbonate transport at this later stage of enamel development.

Changes to NCX1 and NCX3 expression

The role of NCX1 and NCX3 in ameloblasts has been discussed previously, and both localize to the apical poles of polarized ameloblasts indicating that both are involved with the extrusion of Ca^{2+} from enamel cells into the enamel matrix during enamel mineralization (Okumura et al., 2010). The data we present here show that both NCX1 and NCX3 are clearly expressed during amelogenesis with mRNA copy numbers similar to that seen for AE2 and Cftr (Fig. 6). Of note however is that neither gene transcript showed any significant up-regulation during the maturation stages of amelogenesis. Comparing the secretory stage to both the early-mid and mid-late maturation stages, expression of NCX1 remained constant while NCX3 was down-regulated. This may suggest there are additional Ca^{2+} exporters localized at the apical pole of ameloblasts that could play an important role in amelogenesis.

Changes to Car2, Car3, Car6, and Car12 expression

Using CA isoform-specific qPCR primer pairs to all of the known rat CAs (Table 1; note that Car10 has not been identified in the rat genome to date), mRNA for all the isozymes (biologically active CAs) was detected as previously reported by RT-PCR (Lacruz et al., 2010a), however, by qPCR there was a greater appreciation of the levels of expression and the levels of Car2, Car3, Car5b, Car6, Car12, and Car13 (Fig. 7, Part A) which were significantly more highly expressed than other CA isozymes (Car1, Car4, Car5a, Car7, Car9, Car14, and Car15: data not shown), including the non-catalytically active CARP Car 8, Car11, Ptprb, and Ptprg (Wary et al., 1993; Peles et al., 1995; Supuran, 2008a; Fig. 7, Part B). The most up-regulated CAs during the maturation stages are Car2 and Car6, followed by Car3 and Car12 (Fig. 7, Part A). Of note is the expression pattern of Car6 that is essentially absent from the enamel organ in the secretory stage, but transcription is abruptly turned on during the early maturation stage of amelogenesis (Fig. 7, Part A). Of the CA isozymes up-regulated during enamel maturation there are examples of cytoplasmic (Car2 and Car3), plasma membrane-bound (Car12), secreted (Car6), and mitochondrial (Car5b) CAs, suggesting the significance of CA in later stages of enamel maturation.

Discussion

Acidic extracellular environments affect mineralization by potentially preventing crystal growth. Under these conditions, the cells in the immediate vicinity of the growing crystals must provide a buffering mechanism against low pH. The production and movement of HCO_3^- is one such buffering mechanism used commonly by both vertebrates (Tashian, 1989; Fujikawa-Adachi et al., 1999; Chegwidden et al., 2000; Supuran, 2008a,b) and invertebrates (Istin and Girard, 1970; Nielsen and Frieden, 1972; Henry, 1987a,b; Miyamoto et al., 1996; Lee et al., 2008; Marie et al., 2008; Marin et al., 2008; Clark et al., 2010) in the mineralization of their skeletons or exoskeletons. Because our interest here focuses on HCO_3^- production and transport, the ensemble of genes under study is broad. However, their functions are likely interlinked in regulating enamel mineralization. Thus, they should be viewed as an interconnected network of genes engaged at various levels of enamel mineralization.

With this knowledge, we have used rat mandibular incisors to obtain enamel organ cells responsible for either secreting the enamel organic matrix (secretory stage amelogenesis) or for directing mineralization of this “preformed” organic matrix (maturation stage amelogenesis). Cells derived from secretory, early-mid maturation, and mid-late maturation were processed for qPCR analysis. Results for known enamel-specific genes (Amelx, Enam, and Odam; Fig. 5) suggest that our pooled mRNA samples (collected from 10 male adult rats) truly represent the three distinct regions of investigation. This dissection approach allows us to confidently analyze gene activities by examining relative RNA levels at various stages of amelogenesis. In this study, we focus on defining gene activities (transcriptome analysis) involved with pH regulation and ion transport. Genes selected are involved with HCO_3^- transport and synthesis, or Ca^{2+} export, and had been previously identified as products of ameloblast cells. This study shows that the majority of the genes analyzed were significantly up-regulated during enamel maturation, and these data are summarized in Figure 8 (including statistical analyses). The significance of this finding is that multiple molecular activities involved in pH maintenance are up-regulated during enamel maturation, a time when the generation of H^+ is at a peak, and buffering against an acidic environment is critical. In animal and human populations, mutations to many of these genes result in a wide range of systemic diseases such as pRTA, CF, and osteopetrosis. Such diseases frequently include an enamel phenotype.

NBCe1 (encoded by *SLC4A4*) is a Na^+-HCO_3^- transporter, and patients with aberrant NBCe1 expression present with familial pRTA due to a lower than normal level of circulating bicarbonate (Pushkin and Kurtz, 2006). These patients frequently present with skeletal and ocular defects (Demirci et al., 2006; Katzir et al., 2008). Enamel abnormalities have also been identified in patients with inherited pRTA (Koppang et al., 1984; Demirci et al., 2006; Elizabeth et al., 2007); whereas mice null for *Slc4a4* have completely abnormal enamel (Gawenis et al., 2007; Lacruz et al., 2010b,c). In this study, we report marked differences in mineral content between NBCe1 $^{-/-}$ mice and WT littermates, with lower levels of Na^+, Ca^{2+}, P^{3-}, and Cl^- in NBCe1 $^{-/-}$ mice compared to WT controls. The enamel of NBCe1 $^{-/-}$ mice also lacks clear rod–interrod boundaries and presents abnormally packed crystals (Fig. 4). AE2 (encoded by *SLC4A2*) is an anion exchanger (HCO_3^-) and Cl^-, and mice null for the *Slc4a2* gene locus have abnormal enamel (Gawenis et al., 2004; Lyaruu et al., 2008). These clinical and animal observations suggest that both NBCe1 and AE2 each play an essential role in enamel formation (Lacruz et al., 2010b; Urzua et al., 2011). AE1 (encoded by *SLC4A1*) mutations result in red blood cell abnormalities and distal renal tubular acidosis in humans and mice (Bruce et al., 1993, 1997). In humans and mice, NHE1 (encoded by *SLC9A1*) mutations are thought to result in essential hypertension and central nervous system abnormalities (Dudley et al., 1990; Xue et al., 2003; Nakamura

et al., 2008). To the best of our knowledge, in the literature to date, no dental abnormalities have been reported as a result of mutations to these two proteins (AE1 and NHE1) in either humans or mouse models.

AE2 and Cftr are frequently co-expressed in cells where the passive movement of Cl^- into, and out of, cells is required (Shumaker and Soleimani, 1999; Shumaker et al., 1999; Banales et al., 2008; Bronckers et al., 2010; Simmer et al., 2010). The *Cftr*-null mice and the *Slc4a2*-null mice have an enamel phenotype described as hypomineralized with disrupted prismatic structure (Arquitt et al., 2002; Lyaruu et al., 2008). Data from the CF mouse (targeted knockout of the *Cftr* gene locus; Snouwaert et al., 1992) suggest that disruptions to *Cftr* activity impacts on the enamel phenotype (Wright et al., 1996a,b; Sui et al., 2003). CF is the most common life-shortening autosomal recessive disease amongst people of European descent (Welsh, 1990; Welsh and Smith, 1993). Although there are over 1,000 mutations associated with CF, the most common human mutation causing this disease is a deletion of three nucleotides resulting in the loss of a phenylalanine in the protein at position 508 (Kerem et al., 1989; Welsh, 2010). In the U.S., ΔF508 mutations account for nearly 90% of CF cases whereas worldwide ΔF508 mutations account for ~70% (Welsh, 2010). CF porcine models (*Cftr*-null or *Cftr*-ΔF508; Rogers et al., 2008a,b; Stoltz et al., 2010) display a severely hypomineralized enamel of the primary (or deciduous) dentition, which forms in uterus and is partially erupted at birth (Chang et al., 2011). This mineral deficiency and abnormal crystal growth is confirmed in this study in the permanent dentition of *Cftr*-ΔF508 pigs (Fig. 3). The hypomineralization observed in these CF porcine models may be associated with the inability of ameloblasts to process extracellular matrix during maturation, as has been proposed for the mouse CFTR phenotype (Wright et al., 1996a). However, there are a few documented cases that have identified enamel anomalies associated with CF in humans (Primosch, 1980; Narang et al., 2003; Azevedo et al., 2006; Atar and Korperich, 2010; Lacruz et al., 2010b).

Data linking CA mutations to human disease are rare. Patients with CA2 deficiency may, in addition to osteopetrosis that is a typical feature of *CA2* mutations (refer Online Mendelian Inheritance in Man, or OMIM: www.ncbi.nlm.nih.gov/entrez/) show dental abnormalities including hypoplasia, caries, and irregular-shaped teeth (Strisciuglio et al., 1990; Nagai et al., 1997; Awad et al., 2002). Disease states resulting from mutations to other CA genes have not been reported to date.

Sodium–calcium exchangers have been discussed and in the literature (Smith, 1998; Hubbard, 2000), and only recently has it been shown that NCX1 and NCX3, but not NCX2, play a significant function related to Ca^{2+} extrusion during all stages of amelogenesis (Okumura et al., 2010). Our data confirm these earlier findings of Okumura et al. (2010). In addition, our data suggest that NCX1 plays just as an important role during the secretory stage of amelogenesis as it does during the maturation stages, while NCX3 is most highly expressed during the secretory stage with negligible levels detected during the maturation stages. With the significant increase in Ca^{2+} movement into the enamel matrix during the stages of mineralization, as opposed to the secretory stage, the data presented here may be suggestive that additional plasma membrane channels are present to facilitate this movement. This may be achieved by either PMCA1 or PMCA4 as previously discussed (Salama et al., 1987; Borke et al., 1995; Okumura et al., 2010), or as yet to be identified members of the solute carrier family (SLC genes) may be involved.

Ameloblasts are epithelially derived cells responsible for synthesizing enamel matrix, which becomes a hydroxyapatite-based, highly mineralized (~95% by weight mineral content when fully mature) bioceramic with extraordinary mechanical properties (Smith, 1998; White et al., 2000, 2001, 2005; Bartlett et al., 2006). Expression of many of the genes discussed, that

is, AE2, NBCe1, and CFTR are limited to epithelial cells, such as kidney tubular cells (Pushkin and Kurtz, 2006; Gross and Meye, 2008), pancreatic duct cells (Shumaker and Soleimani, 1999; Shumaker et al., 1999; Novak et al., 2010), and tracheal epithelial cells (Wheat et al., 2000) of non-mineralizing tissues and organs, and not widely known to be expressed at significant levels in bone or dentine. Thus, it is remarkable to identify enamel epithelial cells, cells that generate the most highly mineralized tissue in vertebrate biology, utilize the same molecular and biochemical activities as many non-mineralizing tissues involved with ion retention and secretion. In addition, enamel cells have only one opportunity to produce a functional enamel organ that is required to perform during the entire life span of that organism. Failure to fully mineralize enamel during development results in a compromised tooth surface post-eruption. This likely causes greater susceptibility to wear and decay potentially affecting the overall health of the individual.

Conclusion

Stringent control of acid/base homeostasis and ion transport is essential for the development of healthy enamel. To achieve this, the enamel epithelial cells express many pH regulatory genes that modulate this process. We have shown that expression levels of a variety of genes involved with bicarbonate-related transport increase during maturation stage amelogenesis. It is also known that animal models and human pedigrees with mutations to these genes form enamel that is inferior quality thus compromising the animal's longevity. Ion transport is a poorly understood process in enamel biology and pathology, and data presented here highlight the important role of ion transport and bicarbonate generation in enamel formation. The results suggest that there are both developmental and clinical aspects that need to be considered when patients present with specific systemic disease states such as CF or proximal renal tubular acidosis.

Acknowledgments

The authors would like to thank Malcolm L. Snead (University of Southern California, USA) for valuable discussions on this topic and support of the project. The authors also thank Dr. Gary E. Shull (Department of Molecular Genetics, Biochemistry and Microbiology, University of Cincinnati College of Medicine, Cincinnati, Ohio) for providing breeding pairs of NBCe1$^{+/-}$ mice. This work was supported by grants DE013404 and DE019629 (to M.L.P.), DK058563 and DK077162 (to I.K.), HL051670 and HL091842 (to M.J.W.) from the National Institutes of Health, and from the Cystic Fibrosis Foundation (to M.J.W.) and the Canadian Institutes of Health Research (to A.N.).

Contract grant sponsor: NIH;

Contract grant numbers: DE013404, DE019629, DK058563, DK077162, HL051670, HL091842.

Contract grant sponsor: Cystic Fibrosis Foundation.

Contract grant sponsor: Canadian Institutes of Health Research.

Abbreviations

AE1	anion exchanger 1
AE2	anion exchanger 2
BSE-SEM	backscattered electron imaging-scanning electron microscopy
CFTR	cystic fibrosis transmembrane conductance regulator
pRTA	proximal renal tubular acidosis
NBCe1	sodium bicarbonate co-transporter

NHE1	sodium/hydrogen exchanger
qPCR	quantitative real-time PCR.

Literature Cited

Aramaki S, Yoshida I, Yoshino M, Kondo M, Sato Y, Noda K, Jo R, Okue A, Sai N, Yamashita F. Carbonic anhydrase II deficiency in three unrelated Japanese patients. J Inherit Metab Dis. 1993; 16:982–990. [PubMed: 8127074]

Arquitt CK, Boyd C, Wright JT. Cystic fibrosis transmembrane regulator gene (CFTR) is associated with abnormal enamel formation. J Dent Res. 2002; 81:492–496. [PubMed: 12161463]

Atar M, Korperich EJ. Systemic disorders and their influence on the development of dental hard tissues: A literature review. J Dent. 2010; 38:296–306. [PubMed: 20004698]

Awad M, Al-Ashwal AA, Sakati N, Al-Abbad AA, Bin-Abbas BS. Long-term follow up of carbonic anhydrase II deficiency syndrome. Saudi Med J. 2002; 23:25–29. [PubMed: 11938359]

Azevedo TD, Feijo GC, Bezerra AC. Presence of developmental defects of enamel in cystic fibrosis patients. J Dent Child (Chic). 2006; 73:159–163. [PubMed: 17367033]

Banales JM, Masyuk TV, Bogert PS, Huang BQ, Gradilone SA, Lee SO, Stroope AJ, Masyuk AI, Medina JF, LaRusso NF. Hepatic cystogenesis is associated with abnormal expression and location of ion transporters and water channels in an animal model of autosomal recessive polycystic kidney disease. Am J Pathol. 2008; 173:1637–1646. [PubMed: 18988797]

Bartlett JD, Ganss B, Goldberg M, Moradian-Oldak J, Paine ML, Snead ML, Wen X, White SN, Zhou YL. Protein–protein interactions of the developing enamel matrix. Curr Top Dev Biol. 2006; 74:57–115. [PubMed: 16860665]

Borke JL, Zaki Ae-M, Eisenmann DR, Mednieks MI. Localization of plasma membrane Ca^{2+} pump mRNA and protein in human ameloblasts by in situ hybridization and immunohistochemistry. Connect Tissue Res. 1995; 33:139–144. [PubMed: 7554945]

Bronckers AL, Lyaruu DM, Jansen ID, Medina JF, Kellokumpu S, Hoeben KA, Gawenis LR, Oude-Elferink RP, Everts V. Localization and function of the anion exchanger Ae2 in developing teeth and orofacial bone in rodents. J Exp Zool B Mol Dev Evol. 2009; 312B:375–387. [PubMed: 19206174]

Bronckers A, Kalogeraki L, Jorna HJ, Wilke M, Bervoets TJ, Lyaruu DM, Zandieh-Doulabi B, Denbesten P, de Jonge H. The cystic fibrosis transmembrane conductance regulator (CFTR) is expressed in maturation stage ameloblasts, odontoblasts and bone cells. Bone. 2010; 46:1188–1196. [PubMed: 20004757]

Bruce LJ, Kay MM, Lawrence C, Tanner MJ. Band 3 HT, a human red-cell variant associated with acanthocytosis and increased anion transport, carries the mutation Pro-868→Leu in the membrane domain of band 3. Biochem J. 1993; 293:317–320. [PubMed: 8343110]

Bruce LJ, Cope DL, Jones GK, Schofield AE, Burley M, Povey S, Unwin RJ, Wrong O, Tanner MJ. Familial distal renal tubular acidosis is associated with mutations in the red cell anion exchanger (Band 3, AE1) gene. J Clin Invest. 1997; 100:1693–1707. [PubMed: 9312167]

Chang EH, Lacruz RS, Bromage TG, Bringas P Jr. Welsh MJ, Zabner J, Paine ML. Enamel pathology resulting from loss of function in the cystic fibrosis transmembrane conductance regulator in a porcine animal model. Cells Tissues Organs. Apr 28.2011 2011. Epub ahead of print.

Chegwidden WR, Dodgson SJ, Spencer IM. The roles of carbonic anhydrase in metabolism, cell growth and cancer in animals. EXS. 2000:343–363. [PubMed: 11268523]

Clark MS, Thorne MA, Vieira FA, Cardoso JC, Power DM, Peck LS. Insights into shell deposition in the Antarctic bivalve *Laternula elliptica*: Gene discovery in the mantle transcriptome using 454 pyrosequencing. BMC Genomics. 2010; 11:362. [PubMed: 20529341]

Demirci FY, Chang MH, Mah TS, Romero MF, Gorin MB. Proximal renal tubular acidosis and ocular pathology: A novel missense mutation in the gene (SLC4A4) for sodium bicarbonate cotransporter protein (NBCe1). Mol Vis. 2006; 12:324–330. [PubMed: 16636648]

Dinour D, Chang MH, Satoh J, Smith BL, Angle N, Knecht A, Serban I, Holtzman EJ, Romero MF. A novel missense mutation in the sodium bicarbonate cotransporter (NBCe1/ *SLC4A4*) causes proximal tubular acidosis and glaucoma through ion transport defects. J Biol Chem. 2004; 279:52238–52246. [PubMed: 15471865]

Dudley CR, Giuffra LA, Tippett P, Kidd KK, Reeders ST. The Na+/H+ antiporter: A “melt” polymorphism allows regional mapping to the short arm of chromosome 1. Hum Genet. 1990; 86:79–83. [PubMed: 1979310]

Elizabeth J, Lakshmi Priya E, Umadevi KM, Ranganathan K. *Amelogenesis imperfecta* with renal disease—A report of two cases. J Oral Pathol Med. 2007; 36:625–628. [PubMed: 17944757]

Fujikawa-Adachi K, Nishimori I, Taguchi T, Onishi S. Human mitochondrial carbonic anhydrase VB. cDNA cloning, mRNA expression, subcellular localization, and mapping to chromosome X. J Biol Chem. 1999; 274:21228–21233. [PubMed: 10409679]

Gawenis LR, Ledoussal C, Judd LM, Prasad V, Alper SL, Stuart-Tilley A, Woo AL, Grisham C, Sanford LP, Doetschman T, Miller ML, Shull GE. Mice with a targeted disruption of the AE2 $Cl^-/HCO3^-$ exchanger are achlorhydric. J Biol Chem. 2004; 279:30531–30539. [PubMed: 15123620]

Gawenis LR, Bradford EM, Prasad V, Lorenz JN, Simpson JE, Clarke LL, Woo AL, Grisham C, Sanford LP, Doetschman T, Miller ML, Shull GE. Colonic anion secretory defects and metabolic acidosis in mice lacking the NBC1 Na^+/(HCO3−) cotransporter. J Biol Chem. 2007; 282:9042–9052. [PubMed: 17192275]

Gross P, Meye C. Proximal RTA: Are all the charts completed yet? Nephrol Dial Transplant. 2008; 23:1101–1102. [PubMed: 18223262]

Hediger MA, Romero MF, Peng JB, Rolfs A, Takanaga H, Bruford EA. The ABCs of solute carriers: Physiological, pathological and therapeutic implications of human membrane transport proteins introduction. Pflugers Arch. 2004; 447:465–468. [PubMed: 14624363]

Henry RP. Invertebrate red blood cell carbonic anhydrase. J Exp Zool. 1987a; 242:113–116. [PubMed: 3110365]

Henry RP. Membrane-associated carbonic anhydrase in gills of the blue crab *Callinectes sapidus*. Am J Physiol. 1987b; 252:R966–R971. [PubMed: 3107406]

Hu JC, Sun X, Zhang C, Simmer JP. A comparison of enamelin and amelogenin expression in developing mouse molars. Eur J Oral Sci. 2001; 109:125–132. [PubMed: 11347656]

Hubbard MJ. Calcium transport across the dental enamel epithelium. Crit Rev Oral Biol Med. 2000; 11:437–466. [PubMed: 11132765]

Igarashi T, Inatomi J, Sekine T, Cha SH, Kanai Y, Kunimi M, Tsukamoto K, Satoh H, Shimadzu M, Tozawa F, Mori T, Shiobara M, Seki G, Endou H. Mutations in SLC4A4 cause permanent isolated proximal renal tubular acidosis with ocular abnormalities. Nat Genet. 1999; 23:264–266. [PubMed: 10545938]

Inatomi J, Horita S, Braverman N, Sekine T, Yamada H, Suzuki Y, Kawahara K, Moriyama N, Kudo A, Kawakami H, Shimadzu M, Endou H, Fujita T, Seki G, Igarashi T. Mutational and functional analysis of SLC4A4 in a patient with proximal renal tubular acidosis. Pflugers Arch. 2004; 448:438–444. [PubMed: 15085340]

Istin M, Girard JP. Carbonic anhydrase and mobilisation of calcium reserves in the mantle of lamellibranchs. Calcif Tissue Res. 1970; 5:247–260. [PubMed: 4988459]

Josephsen K, Takano Y, Frische S, Praetorius J, Nielsen S, Aoba T, Fejerskov O. Ion transporters in secretory and cyclically modulating ameloblasts. A new hypothesis for cellular control of preeruptive enamel maturation. Am J Physiol Cell Physiol. 2010; 299:C1299–C1307. [PubMed: 20844245]

Katzir Z, Dinour D, Reznik-Wolf H, Nissenkorn A, Holtzman E. Familial pure proximal renal tubular acidosis—A clinical and genetic study. Nephrol Dial Transplant. 2008; 23:1211–1215. [PubMed: 17881426]

Kerem BS, Buchanan JA, Durie P, Corey ML, Levison H, Rommens JM, Buchwald M, Tsui LC. DNA marker haplotype association with pancreatic sufficiency in cystic fibrosis. Am J Hum Genet. 1989; 44:827–834. [PubMed: 2567116]

Koppang HS, Stene T, Solheim T, Larheim TA, Winsnes A, Monn E, Stokke O. Dental features in congenital persistent renal tubular acidosis of proximal type. Scand J Dent Res. 1984; 92:489–495. [PubMed: 6597532]

Lacruz RS, Hilvo M, Kurtz I, Paine ML. A survey of carbonic anhydrase mRNA expression in enamel cells. Biochem Biophys Res Commun. 2010a; 393:883–887. [PubMed: 20175995]

Lacruz RS, Nanci A, Kurtz I, Wright JT, Paine ML. Regulation of pH during amelogenesis. Calcif Tissue Int. 2010b; 86:91–103. [PubMed: 20016979]

Lacruz RS, Nanci A, White SN, Wen X, Wang H, Zalzal SF, Luong VQ, Schuetter VL, Conti PS, Kurtz I, Paine ML. The sodium bicarbonate cotransporter (NBCe1) is essential for normal development of mouse dentition. J Biol Chem. 2010c; 285:24432–24438. [PubMed: 20529845]

Lee SW, Park SB, Choi CS. On self-organized shell formation by bovine carbonic anhydrase II, and soluble protein extracted from regenerated shell. Micron. 2008; 39:1228–1234. [PubMed: 18501616]

Livak KJ, Schmittgen TD. Analysis of relative gene expression data using real-time quantitative PCR and the 2(-Delta Delta C(T)) method. Methods. 2001; 25:402–408. [PubMed: 11846609]

Lyaruu DM, Bronckers AL, Mulder L, Mardones P, Medina JF, Kellokumpu S, Oude Elferink RP, Everts V. The anion exchanger Ae2 is required for enamel maturation in mouse teeth. Matrix Biol. 2008; 27:119–127. [PubMed: 18042363]

Marie B, Luquet G, Bedouet L, Milet C, Guichard N, Medakovic D, Marin F. Nacre calcification in the freshwater mussel *Unio pictorum*: Carbonic anhydrase activity and purification of a 95kDa calcium-binding glycoprotein. Chembiochem. 2008; 9:2515–2523. [PubMed: 18810748]

Marin F, Luquet G, Marie B, Medakovic D. Molluscan shell proteins: Primary structure, origin, and evolution. Curr Top Dev Biol. 2008; 80:209–276. [PubMed: 17950376]

Miyamoto H, Miyashita T, Okushima M, Nakano S, Morita T, Matsushiro A. A carbonic anhydrase from the nacreous layer in oyster pearls. Proc Natl Acad Sci USA. 1996; 93:9657–9660. [PubMed: 8790386]

Moffatt P, Smith CE, St-Arnaud R, Nanci A. Characterization of Apin, a secreted protein highly expressed in tooth-associated epithelia. J Cell Biochem. 2008; 103:941–956. [PubMed: 17647262]

Nagai R, Kooh SW, Balfe JW, Fenton T, Halperin ML. Renal tubular acidosis and osteopetrosis with carbonic anhydrase II deficiency: Pathogenesis of impaired acidification. Pediatr Nephrol. 1997; 11:633–636. [PubMed: 9323296]

Nakamura K, Kamouchi M, Kitazono T, Kuroda J, Matsuo R, Hagiwara N, Ishikawa E, Ooboshi H, Ibayashi S, Iida M. Role of NHE1 in calcium signaling and cell proliferation in human CNS pericytes. Am J Physiol Heart Circ Physiol. 2008; 294:H1700–H1707. [PubMed: 18263712]

Narang A, Maguire A, Nunn JH, Bush A. Oral health and related factors in cystic fibrosis and other chronic respiratory disorders. Arch Dis Child. 2003; 88:702–707. [PubMed: 12876168]

Nielsen SA, Frieden E. Carbonic anhydrase activity in molluscs. Comp Biochem Physiol B. 1972; 41:461–468. [PubMed: 4623971]

Novak I, Wang J, Henriksen KL, Haanes KA, Krabbe S, Nitschke R, Hede SE. Pancreatic bicarbonate secretion: A case for two proton pumps. J Biol Chem. 2010; 286:280–289. [PubMed: 20978133]

Okumura R, Shibukawa Y, Muramatsu T, Hashimoto S, Nakagawa K, Tazaki M, Shimono M. Sodium–calcium exchangers in rat ameloblasts. J Pharmacol Sci. 2010; 112:223–230. [PubMed: 20118617]

Paine ML, Snead ML, Wang HJ, Abuladze N, Pushkin A, Liu W, Kao LY, Wall SM, Kim YH, Kurtz I. Role of NBCe1 and AE2 in secretory ameloblasts. J Dent Res. 2008; 87:391–395. [PubMed: 18362326]

Peles E, Nativ M, Campbell PL, Sakurai T, Martinez R, Lev S, Clary DO, Schilling J, Barnea G, Plowman GD, Grumet M, Schlessinger J. The carbonic anhydrase domain of receptor tyrosine phosphatase beta is a functional ligand for the axonal cell recognition molecule contactin. Cell. 1995; 82:251–260. [PubMed: 7628014]

Primosch RE. Tetracycline discoloration, enamel defects, and dental caries in patients with cystic fibrosis. Oral Surg Oral Med Oral Pathol. 1980; 50:301–308. [PubMed: 6935580]

Pushkin A, Kurtz I. SLC4 base (HCO3−, HCO3−) transporters: Classification, function, structure, genetic diseases, and knockout models. Am J Physiol Renal Physiol. 2006; 290:F580–F599. [PubMed: 16461757]

Rogers CS, Hao Y, Rokhlina T, Samuel M, Stoltz DA, Li Y, Petroff E, Vermeer DW, Kabel AC, Yan Z, Spate L, Wax D, Murphy CN, Rieke A, Whitworth K, Linville ML, Korte SW, Engelhardt JF, Welsh MJ, Prather RS. Production of CFTR-null and CFTR-DeltaF508 heterozygous pigs by adeno-associated virus-mediated gene targeting and somatic cell nuclear transfer. J Clin Invest. 2008a; 118:1571–1577. [PubMed: 18324337]

Rogers CS, Stoltz DA, Meyerholz DK, Ostedgaard LS, Rokhlina T, Taft PJ, Rogan MP, Pezzulo AA, Karp PH, Itani OA, Kabel AC, Wohlford-Lenane CL, Davis GJ, Hanfland RA, Smith TL, Samuel M, Wax D, Murphy CN, Rieke A, Whitworth K, Uc A, Starner TD, Brogden KA, Shilyansky J, McCray PB Jr. Zabner J, Prather RS, Welsh MJ. Disruption of the CFTR gene produces a model of cystic fibrosis in newborn pigs. Science. 2008b; 321:1837–1841. [PubMed: 18818360]

Salama AH, Zaki AE, Eisenmann DR. Cytochemical localization of Ca^{2+}–Mg^{2+} adenosine triphosphatase in rat incisor ameloblasts during enamel secretion and maturation. J Histochem Cytochem. 1987; 35:471–482. [PubMed: 2950164]

Sheppard DN, Welsh MJ. Structure and function of the CFTR chloride channel. Physiol Rev. 1999; 79:S23–S45. [PubMed: 9922375]

Shumaker H, Soleimani M. CFTR upregulates the expression of the basolateral Na(+)–K(+)–2Cl(−) cotransporter in cultured pancreatic duct cells. Am J Physiol. 1999; 277:C1100–C1110. [PubMed: 10600761]

Shumaker H, Amlal H, Frizzell R, Ulrich CD II, Soleimani M. CFTR drives Na^{+}–nHCO-3 cotransport in pancreatic duct cells: A basis for defective HCO-3 secretion in CF. Am J Physiol. 1999; 276:C16–C25. [PubMed: 9886916]

Simmer JP, Fincham AG. Molecular mechanisms of dental enamel formation. Crit Rev Oral Biol Med. 1995; 6:84–108. [PubMed: 7548623]

Simmer JP, Papagerakis P, Smith CE, Fisher DC, Rountrey AN, Zheng L, Hu JC. Regulation of dental enamel shape and hardness. J Dent Res. 2010; 89:1024–1038. [PubMed: 20675598]

Smith CE. Cellular and chemical events during enamel maturation. Crit Rev Oral Biol Med. 1998; 9:128–161. [PubMed: 9603233]

Smith CE, Nanci A. A method for sampling the stages of amelogenesis on mandibular rat incisors using the molars as a reference for dissection. Anat Rec. 1989; 225:257–266. [PubMed: 2683870]

Smith CE, Issid M, Margolis HC, Moreno EC. Developmental changes in the pH of enamel fluid and its effects on matrix-resident proteinases. Adv Dent Res. 1996; 10:159–169. [PubMed: 9206332]

Smith CE, Nanci A, Moffatt P. Evidence by signal peptide trap technology for the expression of carbonic anhydrase 6 in rat incisor enamel organs. Eur J Oral Sci. 2006; 114:147–153. [PubMed: 16674677]

Snouwaert JN, Brigman KK, Latour AM, Malouf NN, Boucher RC, Smithies O, Koller BH. An animal model for cystic fibrosis made by gene targeting. Science. 1992; 257:1083–1088. [PubMed: 1380723]

Stoltz DA, Meyerholz DK, Pezzulo AA, Ramachandran S, Rogan MP, Davis GJ, Hanfland RA, Wohlford-Lenane C, Dohrn CL, Bartlett JA, Nelson GAt, Chang EH, Taft PJ, Ludwig PS, Estin M, Hornick EE, Launspach JL, Samuel M, Rokhlina T, Karp PH, Ostedgaard LS, Uc A, Starner TD, Horswill AR, Brogden KA, Prather RS, Richter SS, Shilyansky J, McCray PB Jr. Zabner J, Welsh MJ. Cystic fibrosis pigs develop lung disease and exhibit defective bacterial eradication at birth. Sci Transl Med. 2010; 2:29–31.

Strisciuglio P, Sartorio R, Pecoraro C, Lotito F, Sly WS. Variable clinical presentation of carbonic anhydrase deficiency: Evidence for heterogeneity? Eur J Pediatr. 1990; 149:337–340. [PubMed: 2107079]

Sui W, Boyd C, Wright JT. Altered pH regulation during enamel development in the cystic fibrosis mouse incisor. J Dent Res. 2003; 82:388–392. [PubMed: 12709507]

Supuran CT. Carbonic anhydrases—An overview. Curr Pharm Des. 2008a; 14:603–614. [PubMed: 18336305]

Supuran CT. Carbonic anhydrases: Novel therapeutic applications for inhibitors and activators. Nat Rev Drug Discov. 2008b; 7:168–181. [PubMed: 18167490]

Tashian RE. The carbonic anhydrases: Widening perspectives on their evolution, expression and function. Bioessays. 1989; 10:186–192. [PubMed: 2500929]

Urzua B, Ortega-Pinto A, Morales-Bozo I, Rojas-Alcayaga G, Cifuentes V. Defining a new candidate gene for *Amelogenesis imperfecta*: From molecular genetics to biochemistry. Biochem Genet. 2011; 49:104–121. [PubMed: 21127961]

Venta PJ, Welty RJ, Johnson TM, Sly WS, Tashian RE. Carbonic anhydrase II deficiency syndrome in a Belgian family is caused by a point mutation at an invariant histidine residue (107 His–Tyr): Complete structure of the normal human CA II gene. Am J Hum Genet. 1991; 49:1082–1090. [PubMed: 1928091]

Wary KK, Lou Z, Buchberg AM, Siracusa LD, Druck T, LaForgia S, Huebner K. A homozygous deletion within the carbonic anhydrase-like domain of the Ptprg gene in murine L-cells. Cancer Res. 1993; 53:1498–1502. [PubMed: 8453613]

Welsh MJ. Abnormal regulation of ion channels in cystic fibrosis epithelia. FASEB J. 1990; 4:2718–2725. [PubMed: 1695593]

Welsh MJ. Targeting the basic defect in cystic fibrosis. N Engl J Med. 2010; 363:2056–2057. [PubMed: 21083391]

Welsh MJ, Smith AE. Molecular mechanisms of CFTR chloride channel dysfunction in cystic fibrosis. Cell. 1993; 73:1251–1254. [PubMed: 7686820]

Wheat VJ, Shumaker H, Burnham C, Shull GE, Yankaskas JR, Soleimani M. CFTR induces the expression of DRA along with Cl(-)/HCO(3)(-) exchange activity in tracheal epithelial cells. Am J Physiol Cell Physiol. 2000; 279:C62–C71. [PubMed: 10898717]

White SN, Paine ML, Sarikaya M, Fong H, Yu Z, Li ZC, Snead ML. Dentino-enamel junction is a broad transitional zone uniting dissimilar bioceramic composites. J Am Ceram Soc. 2000; 83:238–240.

White SN, Luo W, Paine ML, Fong H, Sarikaya M, Snead ML. Biological organization of hydroxyapitite crystallites into a fibrous continuum toughens and controls anisotropy in human enamel. J Dent Res. 2001; 80:321–326. [PubMed: 11269723]

White SN, Miklus VG, Chang PP, Caputo AA, Fong H, Sarikaya M, Luo W, Paine ML, Snead ML. Controlled failure mechanisms toughen the dentino-enamel junction zone. J Prosthet Dent. 2005; 94:330–335. [PubMed: 16198169]

Wright JT, Hall KI, Grubb BR. Enamel mineral composition of normal and cystic fibrosis transgenic mice. Adv Dent Res. 1996a; 10:270–274. [PubMed: 9206347]

Wright JT, Kiefer CL, Hall KI, Grubb BR. Abnormal enamel development in a cystic fibrosis transgenic mouse model. J Dent Res. 1996b; 75:966–973. [PubMed: 8708137]

Xue J, Douglas RM, Zhou D, Lim JY, Boron WF, Haddad GG. Expression of Na+/H+ and (HCO3−)-dependent transporters in Na+/H+ exchanger isoform 1 null mutant mouse brain. Neuroscience. 2003; 122:37–46. [PubMed: 14596847]

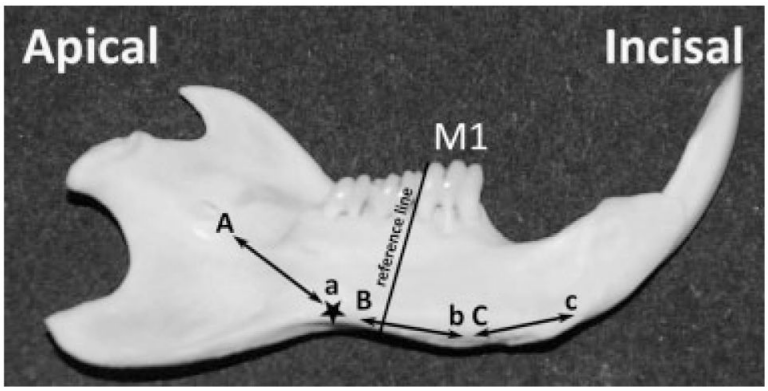

Fig. 1.

Anatomical landmarks guiding the dissection and collection of secretory, early-mid maturation, and mid-late maturation enamel organ cells. The protocol described here has been adapted from the study of Smith and Nanci (1989) for our sample of rats weighing between 170 and 190 g. The study of Smith and Nanci (1989) used a molar reference line (black line apically from M1, and extending perpendicular to the labial aspect of the mandible) to obtain enamel organ cells (largely ameloblasts) from secretory (between “A” and “a”), early maturation (between “B” and “b”) and from late maturation (between “C” and “c”). In our study, the black star marks the position of the end of secretory stage in rats of 170–190 g, about 3 mm apically from the molar reference line. An area of 1 mm incisal to “a” was not collected to avoid possible contamination from post-secretory or transition cells.

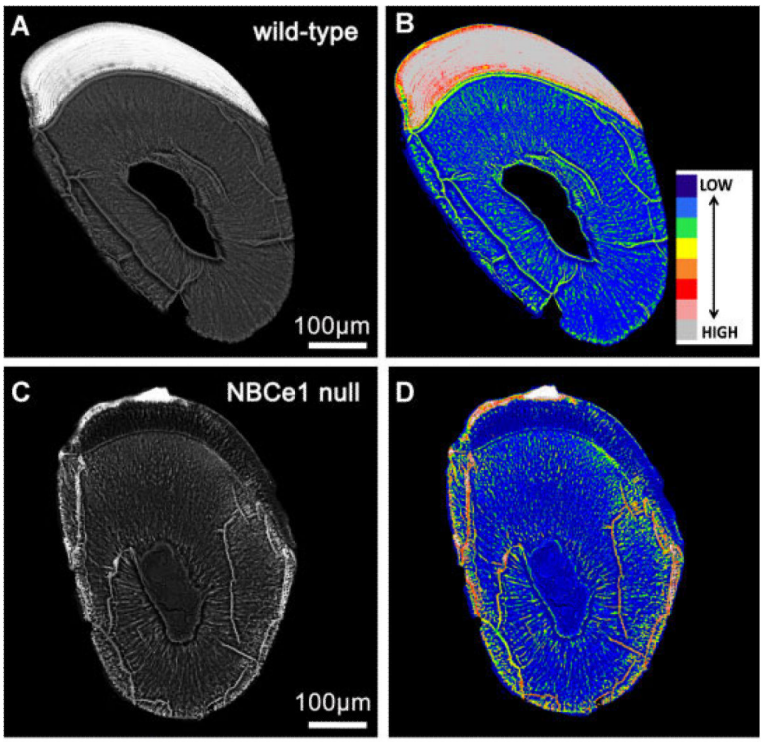

Fig. 2.

BSE-SEM imaging of wild-type (A,B) and NBCe1-null (C,D) mice. Incisor teeth from 14-day-old NBCe1 null mice (Parts C and D) and an age-matched wild-type littermate (Parts A and B) were imaged in BSE-SEM using identical imaging parameters for both, which are defined in the text. Cross-sections are from an erupted, fully mature, region of the tooth. The enamel of the NBCe1-null mice is clearly hypomineralized. This is also evidenced by the color-coded images (Parts B andD), which illustrated marked differences in enamel mineralization for the NBCe1-null mice. Scale bars included.

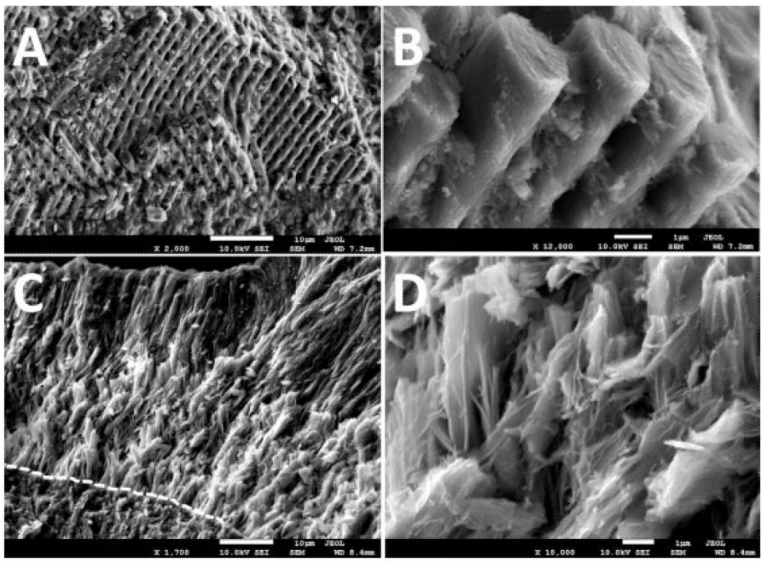

Fig. 3.

FE-SEM imaging. The lower incisors of 15-day-old NBCe1 $^{-/-}$ mice and wild-type littermates were dissected out, air-dried, and mechanically fractured through the mature end (incisal) of the crown using a blade. Specimens were mounted on SEM stubs and carbon-coated for 6 sec to be imaged by FE-SEM. Parts A and B correspond to the enamel of a wild-type mouse, showing normal prisms and clear rod–interrod boundaries. The NBCe1 $^{-/-}$ mice (Parts C and D) lacked normal prismatic structure and present abnormally packed crystals. The EDJ has been highlighted in the NBCe1 $^{-/-}$ animal (dashed line in Part C). Scale bars included.

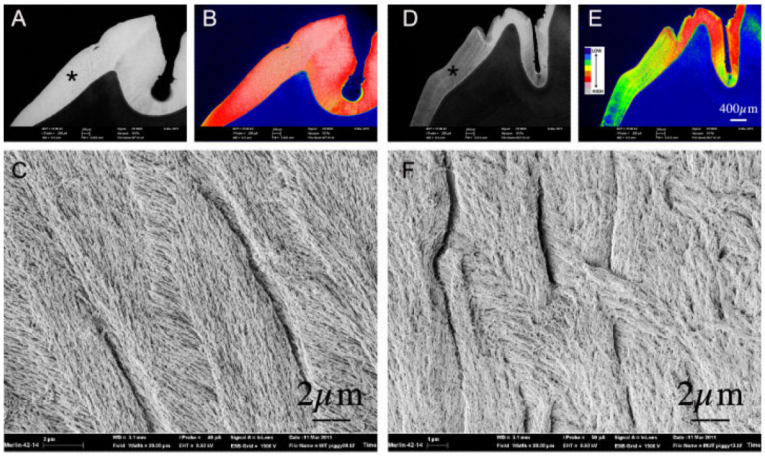

Fig. 4.

BSE-SEM and FE-SEM imaging of the permanent maxillary left first molar of a 6-month-old wild-type domestic pig (Parts A–C) compared toa1 2-month-old cystic fibrosis (*Cftr*-DF508) pig (PartsD–F).Low magnification BSE-SEM images of WT and *Cftr*-DF508 molars are provided in Parts A and D, respectively, both images of which were acquired under identical signal intensity settings. Scale for both is included in Part D. These images were subject to an 8-bin color look-up-table (Parts B and E) for visual comparison to represent differences in mineralization density between samples (see color code insert: wherein cool colors—blue, green, yellow denote lower mineralization density and hot colors—gray, pink, red represent higher mineralization densities). Asterisks on Parts A and D indicate areas shown in Parts C and F imaged at higher magnification (FW = 20 μm) by FE-SEM. Parts C and F represent WT and *Cftr*-DF508 molars, respectively, showing abnormal crystal growth in the latter as imaged in secondary electron emission mode.

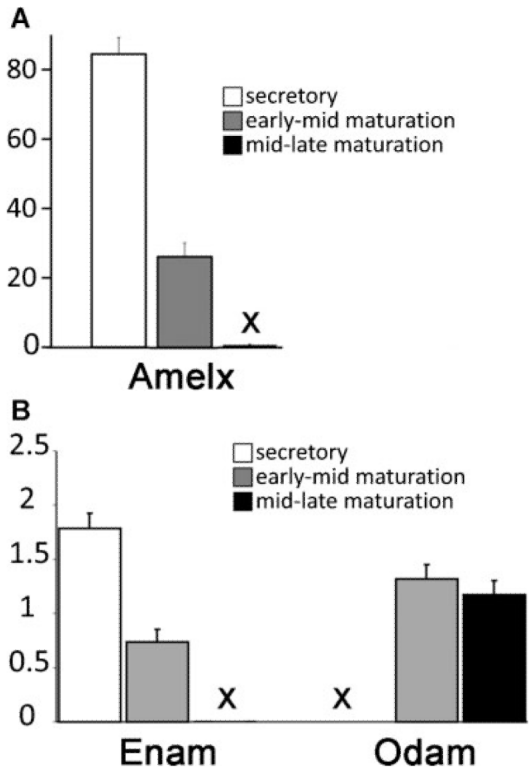

Fig. 5.

Transcript analysis for Amelx (Part A), and Enam and Odam (Part B). The (X) in Parts A and B indicate that the measurements are present but negligible, with no appreciable error bars. The mRNA transcript levels were normalized to those of β-actin. Amelx and Enam expression clearly diminish at the onset of maturation, becoming almost completely absent as maturation progresses. The opposite is observed for Odam. These patterns are entirely consistent with reports on the activity levels of these genes using other methods. Therefore, we conclude that the dissected cells of the enamel organ analyzed in this study are well suited to investigate the expression levels of SLC genes and carbonic anhydrases.

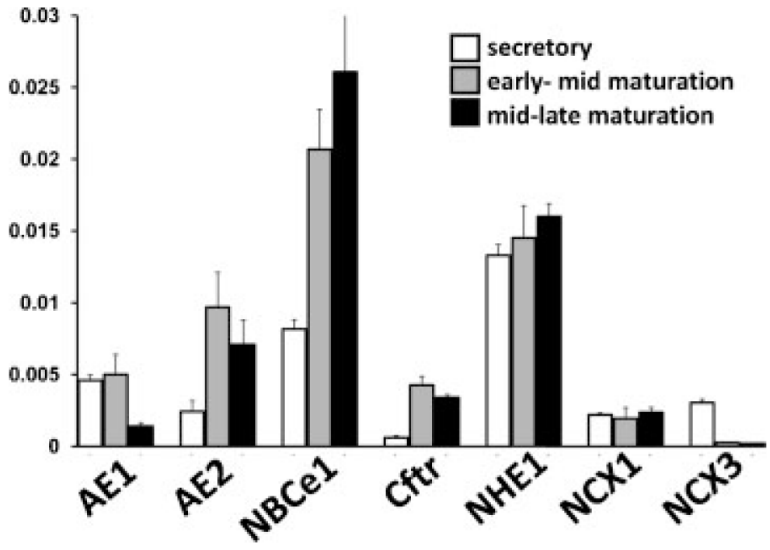

Fig. 6.

Transcript analysis for AE1, AE2, NBCe1, Cftr, NHE1, NCX1 and NCX3. Note that the relative levels of AE1, AE2, NBCe1, Cftr, and NHE1 are of two orders of magnitude less than seen for Enam and Odam (Fig. 5). The mRNA transcript levels were normalized to those of β-actin.

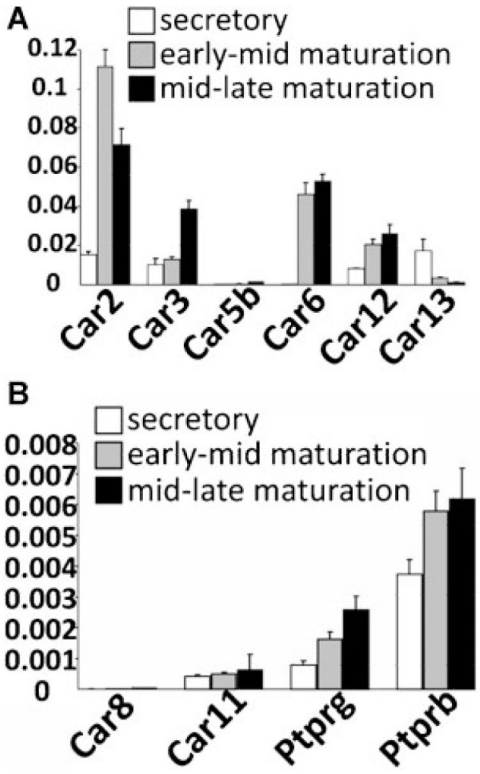

Fig. 7.

Transcript analysis for selected carbonic anhydrases (Part A) and carbonic anhydrase-related proteins (Part B). Note that the relative levels of Car2, Car3, Car6, and Car12 are one order of magnitude less than seen for Enam and Odam (Fig. 5). While levels for Car5b (Part A), and the CA-RPs (Car8, Car11, Ptprg, and Ptprb) were recorded, the levels were low and negligible, as were the transcript levels for Car1, Car4, Car5a, Car7, Car9, Car14, and Car15 (data not included). The mRNA transcript levels were normalized to those of β-actin.

A

Gene Product and Symbol	secretory	early-mid maturation	mid-late maturation
AE1	1	1.1	0.303*
AE2	1	3.4*	2.9*
NBCe1	1	2.6*	3.4*
Cftr	1	7.8*	5.6*
NHE1	1	1.05	1.2
NCX1	1	0.885	1.07
NCX3	1	0.084*	0.063*
Car2	1	6.1*	4.7*
Car3	1	1.2	3.7*
Car5a	1	2.1*	3.7*
Car6	1	127.5*	146*
Car12	1	2.6*	3.2*
Car13	1	0.196*	0.069*

B

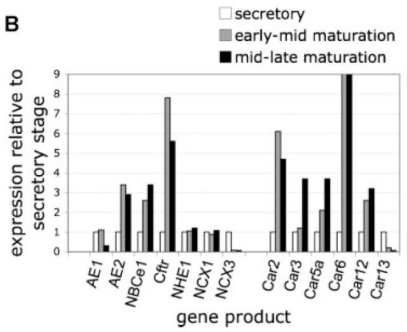

Fig. 8.

Relative levels of enamel epithelial gene up-regulation at early-mid and mid-late maturation stages of amelogenesis when compared to secretory stage amelogenesis, as determined by qPCR. For the selected gene transcripts, levels of both maturation stages were normalized against the level detected during secretory stage. Fold up-regulation is shown, as is the level of down-regulation. Data are presented numerically (Part A) and also as a graph (Part B). A cut-off fold value was used for Car6 in order to illustrate changes in other gene transcripts. Asterisks in Part A indicate statistically significant differences ($P < 0.05$), two-tailed Student's *t*-test comparing secretory versus early-mid maturation or secretory to mid-late maturation stage amelogenesis.

TABLE 1

Rat-specific qPCR primers

Gene	GenBank Ref.	Primer name	Sequence	Rev. primer	Sequence	Product size
Actb	NM_031144	rActb.f	5′-AGTGTGACGTTGACATCCGTA	rActb.r	5′GCCAGGGCAGTAATCTCCTTCT	112
Gapdh	NM_017008	rGapdh.f	5′-AGGTCGGTGTGAACGGATTTG	rGapdh.r	5′TGTAGACCATGTAGTTGAGGTCA	123
Amelx	NM_019154	rAmelx.f	5′-ATAAGGCAGCCGTATCCTTCC	rAmelx.r	5′GTTGGGTTGGAGTCATGGAGT	208
Enam	NM 017468	rEnam.f	5′-TGCAGAAATACAGCTTCTCCT	rEnam.r	5′CATTGGCATTGGCATGGCA	105
Odam	NM 001044274	rOdam.f	5′-ATCAATTTGGATTTGTACCACA	rOdam.r	5′CGTCGGGTTTATTTCAGAAGTGA	242
AE1 (Slc4al)	NM_012651	rAEl.f	5′-TCAGGTCTATGTAGAGCTGCA	rAEl.r	5′CATCCTCTCGAAGGTTTTCCTC	110
AE2 (Slc4a2)	NM_017 04 8	rAE2.f	5′-AGCCCATCTCCCCCTACAC	rAE2.r	5′AAGGTTGTAACTTCGATGTCCAG	186
NBCel (Slc4a4)	NM_053424	rNBCel.f	5′-AGAACCTCCAAAGAGCCTCCCA	rNBCel.r	5′TCTTCACAGTCACCGTGGCCT	132
NCX1 (Slc8al)	NM_019268	rNCXl.f	5′-CAGCACCATTGTGGGAAGCG	rNCXl.r	5′CAGACCTCCACGACACCAGGA	195
NCX3 (Slc8a3)	NM 078620	rNCX3.f	5′-AACCGAAATGGATGGAACGTG	rNCX3.r	5′GTGTTCACCCAATACTGGCTTT	131
NHE1 (Slc9al)	NM_012 652	rNHEl.f	5′-CATCCTGGTCTTTGGGGAGTC	rNHEl.r	5′TGAGGTGAAGGCTGCGATGAC	193
Cftr	NM 031506	rCftr.f	5′-CTGGACCACACCAATTTTGAGA	rCftr.r	5′GCGTGGATAAGCTGGGGCT	162
Carl	NM_001107660	rCarl.f	5′-CTGGCAATCATTGGGGTTTTG	rCarl.r	5′GGGCTCGTTTTCCCTTAGTTTT	103
Car2	NM_019291	rCar2.f.	5′-ACTGGAACACCAAATATGGGGA	rCar2.r	5′GCAAGGATCAAAGTTAGCAAAG	179
Car3	NM_019291	rCar3.f	5′-GCTCCTTTTAATCACTTCGACC	rCar3.r	5′AGCCACACAATGCACTCCTC	112
Car4	NM 019174	rCar4.f	5′-TACGTGGCCCCCTCTACTG	rCar4.r	5′GCTGGTTCTTCTTACAGTCTCC	115
Car5a	NM 019293	rCar5a.f	5′-AAGCCCTTAGCCATCCTCAG	rCar5a.r	5′CTTCGGGTCATAGACACTA	198
Car5b	NM 001005551	rCar5b.f	5′-ATCGAGCCTTACCTCCACTC	rCar5b.r	5′CAGGGTCATAAACACTGTCCC	102
Car6	NM 001134841	rCar6.f	5′-TGGAGCTACTCAGGGGATGACG	rCar6.r	5′TCCTCTTCACATCGATGGG	100
Car7	NM 001106165	rCar7.f	5′-CACCACTGTTGGGGCTACG	rCar7,r	5′TGATGCTGAGGGACATGCAG	175
Car9	NM 001107956	rCar9.f	5′-AGAACAGGCAAGGTTCCCAC	rCar9.r	5′CCATTGTTGCACAGGCTCAGTTC	226
Carl2	NM 001080756	rCarl2.f	5′-GGGTCCCTGACTACACCTCC	rCarl2.r	5′GGTAAGCAGTCCTTGTCGGAA	219
Carl3	NM 001134993	rCarl3.f	5′-ACCCCAGTTTTGTAGAGGC	rCarl3.r	5′ACCGTGTTTGTTTACCCTTTTCC	144
Carl4	NM 001109655	rCarl4.f	5′-ACACGGTCAGGACCATTGG	rCarl4.r	5′GATCGGGGTCAAATATCACACCG	101
Carl5	NM 001105901	rCarl5.f	5′-CTCTATGGAGATGCACATGGTC	rCarl5.r	5′CCAGACACGATGGCAGAGAAA	147
Car8	NM 001009662	rCar8.f	5′-CAGGGACTGTGAAGTCAC	rCar8.r	5′GGCTTTGAAATTGACCGTATG	175
Carll	NM 175708	rCarll.f	5′-GCAGCTCACATCGGACCCG	rCarll.r	5′GGTCATAAAGAACCCGCTTCA	181
Ptprb	NM 0011080095	rPtprb.f	5′-CTGATGCCTGGACGAAATTAC	rPtprb.r	5′TTGCTGACCTCCAAGTCAGT	119
Ptprq	NM 134356	rPtprq.f	5′-GGCCCGTTCCCATCTCCTAC	rPtprq.r	5′GTGGTCGGAAGTTATTTCTCAGG	111

Gene product, gene symbol, GenBank accession number, and expected product size listed. All primer pairs span intron sequences, and only single products were produced during qPCR. Product sizes are in base pairs. Note that Car10 is not represented in the rat genome.